Materials Research Express

PAPER

Creation of uniformly dispersed nitrogen-vacancy centers in nano-diamonds by low energy ion-irradiation

Ravi Kumar[1,2], **Tai Trinh Cong**[3], **Kwanggeol Lee**[3], **Prabir Pal**[4], **S R Dhakate**[1,2], **Raj Kumar**[5], **Devesh K Avasthi**[6] and **Dilip K Singh**[7]

[1] CSIR-National Physical Laboratory, New Delhi, India-110012
[2] Academy of Scientific and Innovative Research (AcSIR), Ghaziabad, India 201002
[3] Department of Physics, Hanyang University, Seoul, 133-791, Republic of Korea
[4] CSIR-Central Glass and Ceramic Research Institute, Jadavpur, Kolkata 700032, India
[5] Inter University Accelerator Centre, Aruna Asaf Ali Marg, New Delhi-110067, India
[6] Amity Institute of Nanotechnology, Amity University, Noida-201313, India
[7] Department of Physics, Birla Institute of Technology Mesra, Ranchi-835215, India

E-mail: dilipsinghnano1@gmail.com

RECEIVED
7 May 2019

REVISED
2 July 2019

ACCEPTED FOR PUBLICATION
23 July 2019

PUBLISHED
16 October 2019

Keywords: nano-diamonds, nitrogen vacancy centers, fluorescence, ion-irradiation

Supplementary material for this article is available online

Abstract

The inability of the fabrication of uniformly distributed Nitrogen-vacancy (NV) centers in Nano diamonds (NDs) puts serious limitation on their application in bio-medical, sensing and nano-photonics applications. Asymmetry in the concentration of NV centers is mainly due to vacancy generation by single energy ion-irradiation. We report the fabrication of uniform and high concentration of NV centers in NDs using different low energy He^+ ion irradiation. The He^+ ion-irradiation was carried out at different energy range between 10 to 50 keV based on the SRIM simulation for the creation of vacancies. The ion implantation was not found detrimental to the crystallinity of NDs. No sign of intra-crystallite defect patches was found as revealed by x-ray diffraction (XRD). Emission spectra reveal that particular irradiation energy range (40–50 keV) leads to maximum emission intensity from NV centers. Further emission contrast in ZPL of NV^-/NV^o becomes ~2 fold for this energy range. The emission from NV centers (570–670 nm) is relatively uniform and well dispersed for 40–50 keV as revealed by confocal microscopy. This suggests that ion irradiation at 40–50 keV is the optimized ion dose for the fabrication of uniformly dispersed high concentration of NV^- centers in NDs.

Introduction

Nano diamonds (NDs) have inert diamond core, chemically tailorable outer surface and hosts various color centers [1, 2]. These unique properties lead to diverse applications of NDs like optical bio-imaging, drug delivery [3, 4], bio-sensing [5] and quantum information processing [6]. Whereas the other carbon nanomaterials (owing to reactive sp^2 carbon) and inorganic quantum dots (owing to heavy metals) are found to be cytotoxic in different studies, the NDs are perfect bio-compatible as demonstrated with different cell types [7, 8]. The non-cytotoxicity and bio-compatibility of NDs are due to lack of free electrons in NDs owing to sp^3 hybridized carbon atoms. Further, the surface of NDs can be tailored (hydrogenation, oxygen moieties, amino group etc) with ease[2]. The covalent and non-covalent conjugation with a variety of bio-molecules (proteins and peptides) can be achieved easily by surface functionalization [9, 10]. Among different color centers, nitrogen vacancy (NV^-) centers are most desirable fluorophores and quantum probe due to their electronic structure and wide emission range [11]. These centers have substitutional nitrogen atom with adjacent lattice vacancy along any of the ⟨111⟩ crystallographic direction. Additional electron is trapped by NV^o centers (zero phonon line (ZPL) ~ 575 nm) to subsequently form the NV^- centers. The photo-physical properties and relative abundance of NV^- and NV^o centers can be controlled through surface modification [12–14]. The NV^- centers have ZPL at ~637 nm and

emission range is 600–800 nm with high quantum yield ($\phi \sim 1$) [15]. This emission range does not coincide with the fluorescence maxima of different biological molecules like flavins and porphyrins ($\lambda_{em} \sim$ 300–400 nm) [16–18]. The NV^- centers emission has large penetration depth through biological samples. Due to localization of exciton near the color center, NV^- centers are not affected by the surface defects and photo blinking is not occurred [5]. Apart from non-blinking, the NV^- centers do not bleach out even under continuous laser excitation for long time [19]. These features make NDs ideal probe for long time *in vivo* and *in vitro* intra cell tracking of different bio-molecules [20, 21]. The side band emission of NV^- centers (except near the surface) is not prone to the heterogeneous chemical environment of different cells and tissues. The fluorescence resonance energy transfer (FRET) efficiency with NV^- centers as donor (single molecule quencher) has been found to be as high as 95% [22]. Brightness of NV^- centers is much higher as compared to a variety of fluorescent proteins [23] and single molecule dyes [10] owing to their high absorption cross section (5×10^{-17} cm^2). The NV^- centers have triplet ground state ($S = 1$) with the partial splitting of sub states (zero field splitting, $D = 2.87$ GHz) [11]. Optically detected magnetic resonance (ODMR) detection [24, 25] due to Zeeman splitting of ground state (^3A) and optical spin polarization ($m_s = 0$) leads to detection of local magnetic field in intracellular environment by the use of NV^- centers [5]. The NV^- centers may increase the sensitivity of NMR by the transfer of spin polarization to target spin via nitrogen donors [26]. For the application of NDs like bio-imaging, live bio-tracking, ensemble magnetic field sensing and nano-photonics, the high and uniform concentration of NV^- centers through all the crystallites of NDs is desirable.

In situ creation of NV centers in NDs is possible with chemical vapor deposition and sintering of detonation NDs [27, 28]. But, ion-irradiation is most viable method for the fabrication of color centers. NV centers are routinely created in thermally stable substitutional nitrogen (N_s) rich (Type Ib) NDs. The concentration of N_s is generally very high (~100 ppm) but *in situ* concentration of NV centers or vacancies is found to be very low [29]. For vacancy creation, high energy ion irradiation (1–100 MeV) is generally carried out with electrons, protons, helium ions, nitrogen and occasionally with heavier ions [1, 27, 30]. Subsequent vacuum annealing at high temperature (>600 °C) migrates the vacancies through the lattice. The vacancies are trapped by immobile substitutional nitrogen atoms and NV centers are formed. High energy ion irradiation is not efficient for NDs films due to shallow thickness of sample (~0.5 μm) and large penetration depth of high energy ions. The electronic energy losses dominate near the surface and negligible vacancies are created in NDs films. Most of the vacancies (nuclear energy losses) are concentrated near the end range [31, 32]. The crystallites containing higher concentration of lattice vacancies have much higher probability of formation of NV^o centers as compared to NV^- centers due to limited concentration of substitutional nitrogen atoms (electron donars). High concentration of NV^o centers near the penetration depth limit and much lower concentration of NV centers near the surface of NDs limit the usability of NDs. This put the severe limitation on high energy ion-implantation for the vacancy generation. Further, the high energy experiments require complicated accelerator machinery and make the commercial production of NV centers financially unviable through high energy ion-irradiation. Tse-Luen Wee *et al* have compared the fluorescence intensity (confocal microscopy) of high (3 MeV, 14 vacancies/ion) and low energy protons (40 keV, 4 vacancies/ion) [33]. The emission intensity is almost doubled for high energy ion irradiation. Chang *et al* have shown that the emission from NDs irradiated with high energy protons (3 MeV, H^+) and low energy helium ions (40 keV, He^+) has same spectral features [34]. The sample irradiated with high energy was found to have emission contrast of only ~30% as compared to low energy He^+ ions. Subsequently, the low energy He^+ ions have been routinely implanted for vacancy creation in NDs [9, 35, 36]. Helium ions are best suited for vacancy generation due to their chemical inertness and generation of large number of vacancies per ion through the lattice. Huan-Cheng Chang *et al* have reported the irradiation of NDs with low energy He^+ ions (40 keV) for 3–4 times (by scratching the sample each time from flat substrate and recoat it) to achieve some uniformity in creation of NV centers [36]. This method leads to repetitive irradiation of certain parts and phase change may occur due to overexposure. Peter Cigler *et al* have reported the use of high energy ion-irradiation (MeV, protons) to fabricate uniform NV centers in colloidal solution of NDs [37]. High energy irradiation and liquid chamber for irradiation makes it complicated and unviable method for creation of NV centers. A systematic experiment using low energy H^+ ion, He^+ ion and Li-ion has established the superiority of 60 or, 80 keV (10^{13} dose) for production of high quality NDs containing NV^- centers using optically detected magnetic resonance (ODMR) and Raman spectroscopy measurements [38]. In our recent work, we have showed that irradiation at 50 keV and 10^{13} dose produces bright fluorescence [39]. Surprisingly, in spite of numerous application of NV^- NDs, the uniformity of NV centers per particles is not yet achieved. In literature, there is no systematic study on the optimization of ion-irradiation conditions for uniform dispersion of NV centers through NDs. For the efficient use of NDs for any application, uniformity of NV centers and their high concentration are urgently required.

In the present work, we have optimized the fabrication conditions for uniform distribution of NV centers in NDs through different low energy ion irradiation (10–50 keV). Minimum structural damage and maximum uniformity of NV color centers have been investigated through different He^+ ion irradiation conditions.

Table 1. Effect of He^+ ion-energy and dose on formation of vacancies in NDs.

Sample name	Ion energy (KeV)	Dose (10^{12} (Ions/cm^2)	Effec. dose	Range (nm)	Avg. range (nm)	Vacancies per ion	Total ($\times 10^{14}$)	(ppm)	per 20 nm cryst.
ND35R8HCl 10–20 keV	10	3.33		52.4		20			
	15	3.33	10^{13}	73.7	73.2	24	2.33	181.0	25.5
	20	3.33		93.5	± 16.8	26			
ND35R8HCl 20–30 keV	20	3.33		93.5		26			
	25	3.33	10^{13}	111.4	111.1	28	2.93	149.9	21.1
	30	3.33		128.4	± 14.2	30			
ND35R8HCl 30–40 keV	30	3.33		128.4		30			
	35	3.33	10^{13}	144.6	144.3	31	3.097	122.0	17.2
	40	3.33		160	± 12.9	32			
ND35R8HCl 40–50 keV	40	3.33		160		32			
	45	3.33	10^{13}	174.1	173.9	33	3.297	107.8	15.2
	50	3.33		187.7	± 11.3	34			

Reported results establish the fabrication conditions to achieve the uniformly dispersed NV color centers. The maximum contrast between NV^-/NV^o and minimum side band emission has also been achieved for optimized ion irradiation condition. Uniform and high concentration of NV^- centers over NV^o centers has very high potential for bio-imaging, live tracking and ensemble bio-sensing applications.

Experimental

Synthesis of nano-diamonds (NDs) and creation of NV centers

HPHT microdiamonds (element six, MICRON + MDA M0.10) were de agglomerated by salt and water assisted planetary ball milling (35 h, 250 RPM) and acid reflux (H_2SO_4:HNO_3 in 3:1 ratio at 80 °C for 8 h). The purification method has been given in our previous work [40]. Water dispersed purified NDs (ND35R8HCl) were drop casted on silicon wafers (1 cm × 1 cm) to prepare NDs thin films (~0.5 μm) on Si wafers. He^+ ion irradiation was carried out with custom built table top ion accelerator (IUAC 50 keV ion accelerator) at IUAC New Delhi, India. Four different He^+ ion beam conditions (table 1) were used for the creation of vacancies in NDs. Irradiated NDs were vacuum annealed (rotary) at 750 °C for 2 h [39]. Annealed NDs were subsequently oxidized in ambient air flow at 450 °C for 2 h [41]. In this way, fluorescent NDs were prepared by different ion irradiation conditions with varying energy range for each irradiation. Post-irradiation NDs were removed from silicon substrate by scratching for measurements.

Characterizations

The degree of de agglomeration and shape of different irradiated NDs have been analyzed using scanning electron microscopy (Model No. VP-EVO, MA-10, Carl-Zeiss, UK). The x-ray diffraction (X'Pert Pro PAN analytical x-ray diffractometer, $2\theta = 20°$ to 80°, scanning rate 0.05 degree/s) of different NDs films has been observed with Cu-K_α ($\lambda = 1.540\,59$ Å). Glancing incidence geometry with incidence angle of 1° is used to characterize NDs thin films. The photoluminescence (PL) and Raman spectra of NDs were observed using Renishaw in Via Raman Microscope having excitation of 514 nm (Ar^+ ion laser). All the spectra were observed in the backscattering geometrical arrangement (single monochromator, 50× objective). Surface analysis of different NDs carried out using x-ray photoelectron spectroscopy (XPS). The XPS was carried out using Omicron μ-metal ultrahigh vacuum (UHV) equipment. The x-ray is generated with monochromatic Al K_α source (resolution 400 meV) having energy of 1486.6 eV. The NDs thin films were placed on sample holder with the help of welded metal (gold) foils. Due to the inherent insulating nature of NDs films, an electrical contact was made between the samples and sample holder to avoid electric charging. Before the measurements, the NDs films were annealed under UHV conditions at 300 °C to remove the surface adsorption of oxygen. The XPS measurements were carried out at room temperature and UHV conditions ($P \sim 5.0 \times 10^{-11}$ mbar). The energy calibrations were carried out by assuming the position of Ag $3d_{5/2}$ at 368.27 eV.

Results and discussion

The average penetration depth of He^+ ions and density of vacancies per ion and per 20 nm crystallite was estimated using stopping and range of ions in matter (SRIM) calculations and are summarized in table 1 [42]. The displacement energy for diamond lattice was taken to be 37.5 eV [along (100) direction] [43]. The plots of He^+ ions profile with varying energy range 10–20 keV, 20–30 keV, 30–40 keV and 40–50 keV is shown in figure S1 is available online at stacks.iop.org/MRX/6/115097/mmedia (Supplementary information). The vacancy concentration at different energy ranges has been calculated by taking the average energy range as the exposed thickness of the sample and multiplying it with beam cross-section area (1 cm $\times$ 1 cm) to find exposed volume of sample. The total number of vacancies created at particular energy range (table 1) are divided the total number of atoms (Substitutional carbon atoms) present in the exposed volume to find the vacancy concentration. Due to the fact that increase in ion beam energy range, there is only marginal increase in the total number of vacancies but drastic increase in the exposed volume as summarized in figure S1 and table 1. The concentration of vacancies thus decreases with the increase in the energy range of ion beam. For irradiation at 10–20 keV, the electronic energy losses are much small and vacancy generation starts near the surface of NDs. The high concentration of vacancies at low energy range is due to the fact the range of He^+ ions is small and vacancies are concentrated in small region of NDs. As the irradiation energy increases, end range increases and the vacancy profile gets distributed over larger region in NDs. This leads to lower vacancy concentration at higher energy range but over distributed range within the particle, not on the outer surface. Vacancy concentration is maximum for 10–20 keV (~181 ppm) and minimum for energy range 40–50 keV (107.8 ppm). The maximum vacancies per crystallite has been created for energy range 10–20 keV (25.5 vacancies/crystallite) and minimum for energy range 40–50 keV (15.2 vacancies/crystallite). The energy range 40–50 keV has the higher probability for preferable fabrication of NV^- centers over NV^o centers. It is due to the fact that lower concentration of vacancies implies the higher concentration of unoccupied paramagnetic substitutional nitrogen atoms (N_s) after the creation of NV centers. Hence, the unoccupied N_s would provide extra electrons to NV^o centers for the creation of NV^- centers. This leads to higher concentration of NV^- centers over NV^o centers. As the vacancy concentration increases, the concentration of unoccupied N_s become smaller after vacuum annealing and the number of extra electrons for creation of NV^- centers become smaller. This hinders the preferable creation of NV^- centers over NV^o centers for low energy ranges.

Figure 1 shows the scanning electron microscopy (SEM) micrographs of sample irradiated with energy range 10–20 keV (figure 1(a)), 20–30 keV (figure 1(b)), 30–40 keV (figure 1(c)) and 40–50 keV (figure 1(d)). Average size of NDs has been calculated using ImageJ software over 30 particles. The average particle size and the standard deviation for different irradiated samples are summarized in table 2. It is clear from the figure that agglomeration has increased in ion irradiated NDs. Average size of the ion irradiated NDs is larger as compared to purified NDs (ND35R8HCl, 70–80 nm). The particle size of sample irradiated with energy range 10–20 keV is widely scattered (Average size 162.3 nm) having standard deviation of 62.9 nm. The agglomeration of NDs for this energy range is due to larger surface modification by lower energy ion beam (10 keV). Functionality of outer surface damaged and non-diamond carbon phases appeared at the outer surface. This leads to inter particle covalent bonding and agglomerates becomes comparable in size to as received NDs (127 $\pm$ 67.9 nm). The agglomeration is persistent for sample irradiated with ion beam energy range of 20–30 keV (figure 1(b), 149.9 $\pm$ 64.8 nm) and 30–40 keV (figure 1(c), 250.8 $\pm$ 76.3 nm). The average particle size (116.1 nm) and standard deviation (39.6 nm) reduces for sample irradiated with energy range 40–50 keV (figure 1(d)).

Figure 2 shows the x-ray diffraction (XRD) pattern of as received sample (ND0), purified (ND35R8HCl), sample irradiated (vacuum annealed and air oxidized subsequently) with energy range 10–20 keV, 20–30 keV, 30–40 keV and 40–50 keV. The (111) peak has been fitted with Voigt line shape (figure S2(c), supplementary information). The crystallite size has been estimated with Scherrer equation [44]. The calculated crystallite size for different NDs is summarized in table 2. As received NDs (ND0) exhibit (111) and (220) diffraction peaks at 43.97° and 75.39° respectively. The crystallite size of ND0 was found to be 19.7 nm. Purification of NDs (ND35R8HCl) does not affect the (111) peak position (43.97°) but the crystallite size is found to be increased (21.9 nm). Sample irradiated with the energy range 10–20 keV exhibits (111) peak at 43.98° (FWHM $\sim$ 0.46°). The crystallite size for this sample (18.7 nm) was nearly same as that of as received NDs (ND0). The crystallite size and the peak position shows that crystallinity is not disturbed due to ion irradiation and defects are mainly localized to the surface. As the concentration of He^+ ions is also small (10^{13} ions cm^{-2}) and dispersed, the possibility of the formation of localized defect patches in the crystalline order is negligible. Sample irradiated with energy 20–30 keV exhibits (111) diffraction peak at 43.98° (FWHM $\sim$ 0.46). The crystallite size (18.8 nm) is also not much changed as compared to initial sample (ND0). Sample irradiated with the energy range 30–40 keV shows the characteristic (111) diffraction peak at 43.97° (FWHM $\sim$ 0.47°). The crystallite size is smaller (18.4 nm) as compared to sample irradiated with energy range 10–20 keV and 20–30 keV. Sample irradiated with energy range 40–50 keV exhibits characteristic (111) peaks at 43.99° (FWHM $\sim$ 0.45°). The

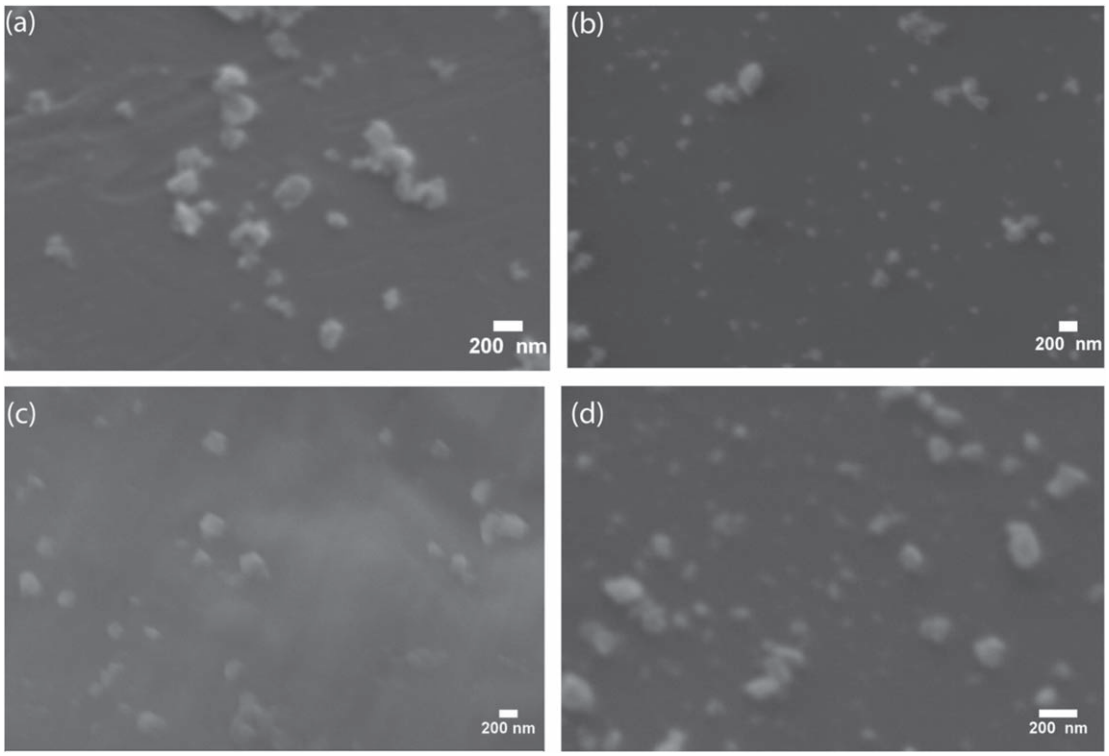

Figure 1. SEM micrographs of different ion irradiated NDs. (a) 10–20 keV, (b) 20–30 keV, (c) 30–40 keV and (d) 40–50 keV. The relative degree of agglomeration is different for varying ion irradiation conditions. 10–20 keV and 30–40 keV ion irradiation conditions lead to more agglomeration as compared to 20–30 keV and 40–50 keV. Agglomeration depends upon the surface reconstruction due to ion beam damage.

Table 2. Variation in crystallite size and particle size with varying energy and ion-dose.

Sample name	Crystallite size (XRD) (nm)	Particle size (SEM) (nm)
ND0	19.7	127.9 ± 67.9
ND35R8HCl	21.8	91.7 ± 31.5
ND35R8HCl 10–20 keV	18.7	162.3 ± 62.9
ND35R8HCl 20–30 keV	18.8	149.9 ± 64.8
ND35R8HCl 30–40 keV	18.4	255.4 ± 90.5
ND35R8HCl 40–50 keV	18.9	116.1 ± 39.6

crystallite size for this sample was found to be 18.9 nm. It is clear from the XRD profile of different ion irradiated NDs that the crystallinity is not affected by low energy ion irradiation. It is due to the dispersed vacancy generation by He^+ ions. Since the vacancies are localized into respective crystallite (~19 nm) their diffusion at elevated temperature (750 °C) are also terminated at the crystallite interface. This leads to generation of surface defects and agglomeration of irradiated NDs (figure 1, SEM). Figure 2(b) shows the Raman spectra of different irradiated samples. Raman spectra for different samples were fitted with Lorentzian line shape (figure S2(b), supplementary information). Fitted data is summarized in table S1. Initial sample (ND0) exhibits large content of graphitic carbon (66.4%) and defects (21.1%) in addition to weak diamond signatures (12.4%). Hence, initial sample have high graphitic carbon at outer surface which surrounds the diamond crystallite. Purification of NDs (ND35R8HCl) leads to suppression of G-band (42.1%) and enhancement of diamond signal (27.3%). Ion irradiation leads to defects creation and detachment of functional groups (electronic energy losses) from the outer surface. For sample irradiated with the energy range 10–20 keV, diamond signal quenches (2.4%) and enhancement in graphitic carbon (54.7%) and defects (42.8%). Diamond signal quenches further (1.1%) for sample irradiated with energy range 20–30 keV and enhancement of graphitic carbon (66.3%) and defects (32.6%). For sample irradiated with the energy range 30–40 keV, diamond signal suppressed further (0.9%) and high amount of graphitic carbon (61.7%) and defects (37.4%). For sample irradiated with the energy range 40–50 keV, the defects (35.5%) and graphitic carbon (63.3%) remain intact in addition to weak diamond signatures (1.2%). As confirmed by XRD, the defects are localized to the surface and crystallinity is intact. The

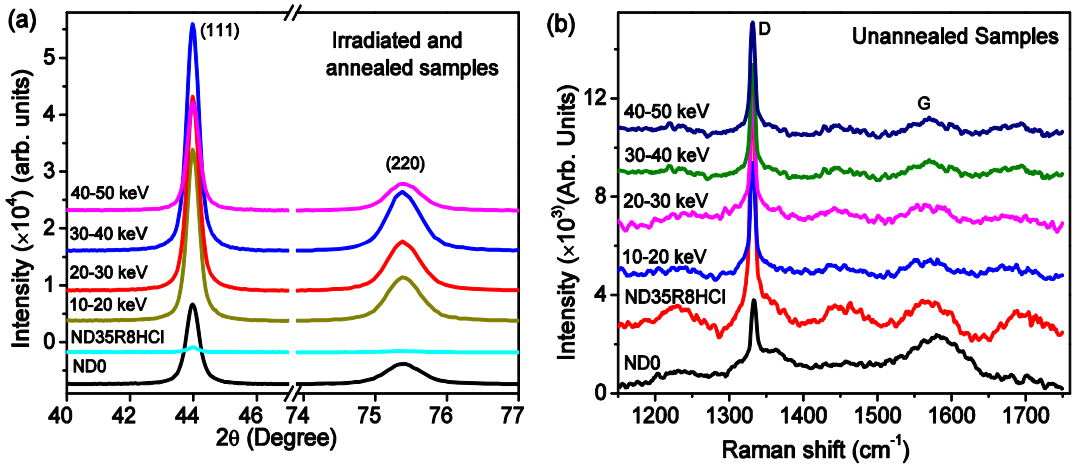

Figure 2. (a) X-ray diffraction (XRD) pattern for as received (ND0), purified (ND35R8HCl) and different ion irradiated NDs. (b) shows the Raman spectra for different irradiated NDs without vacuum annealing. The diamond signal suppressed for ion irradiated NDs as compared to the purified sample (ND35R8HCl).

weaker signal of diamond carbon is due to its lower scattering cross section as compared to graphitic carbon. High concentration of the engineered defects and sp^2 carbon is potential quencher for the emission of NV centers and must be removed before the emission studies to be conducted. The Raman spectra for different ion irradiated, vacuum annealed and subsequently air oxidized NDs is shown in figure S2(a) (supplementary information). Due to strong emission from NV centers, characteristic diamond signal is shadowed. The G bands for different irradiated samples are weaker as compared to purified NDs: ND35R8HCl. Thus air oxidation is found as efficient method for the removal of defects and graphitic content from outer surface [39].

Figure 3 shows the x-ray photoelectron spectroscopy (XPS) analysis of different NDs. Figure 3(a) shows the survey scan for as received (ND0), purified (ND35R8HCl) and different irradiated (vacuum annealed and air oxidized) NDs. The XPS data has been analyzed by Gaussian-Lorentzian line shape fitting with Shirley background subtraction (XPS peak 4.1). Survey scan shows the presence of oxygen (O1*s*) and nitrogen (N1*s*) in addition to carbon (C1*s*) in different NDs. Presence of nitrogen (N_s) is very feeble in all the samples due to the presence of nitrogen atoms at substitutional positions and not near the surface. Initial NDs (ND0) have feeble presence of oxygen. The oxygen peaks are enhanced in purified and ion irradiated NDs. Large presence of oxygen is mainly due to post annealing air oxidation of all the irradiated NDs. Irradiation induced defects are minimized due to air oxidation and oxygen is attached at the outer surface. Figure 3(b) shows C1*s* core spectra for different NDs. The C1*s* core of different NDs is shifted toward higher binding energy as compared to reference value [45]. It is due to insulating nature of diamond. The shape of C1*s* core for all the NDs (except ND0) is asymmetric and broadened toward higher binding energy due to C–O and C=O bonding. Figure 3(c) shows the C1*s* fitted data for ND35R8HCl, 30–40 keV sample. Other samples were analyzed by following same method (table S2, supplementary information). Initial Sample (ND0) contains sp^2 rich outer surface (79.9%) and much smaller presence of diamond sp^3 phase (20.0%). Hence in the probe depth of XPS, much of the sample contains defects and sp^2 carbon. The presence of sp^2 carbon at the outer surface is also confirmed by Raman spectra of as received NDs (G band). Chemical etching of the outer surface leads to drastic reduction of sp^2 carbon near outer surface. In case of ND35R8HCl, sp^2 carbon has been reduced (37.4%) and sp^3 content (24.8%) has been increased. In addition to this, oxygen functional groups (C–O) has been attached due to acid reflux (37.8%). Ion irradiation leads to surface modification and defects in the diamond matrix. Electronic losses caused at the outer surface leads to detachment of the oxygen from the outer surface and formation of the sp^2 carbon phases. Even post annealing air oxidation (450 °C) could not recover completely the oxygen functional groups at the outer surface. It is clearly observed in the ion irradiated NDs. The sp^2 carbon has been increased (54.6%) and surface oxygen functional groups has been reduced (17.3%) in sample irradiated with energy range 10–20 keV. The sp^3 phase has been increased (28.1%) due to surface etching by air oxidation. For the sample irradiated with the energy range 20–30 keV, the sp^2 carbon content is reduced (16%) and surface oxygen increases (27.3%). Further, sp^3 carbon is also increased (56.6%). For sample irradiated with the energy range 30–40 keV, sp^2 carbon (18.2%) is increased, oxygen functional groups are decreased (23.5%) slightly and sp^3 carbon phases are further enhanced (58.2%). For the sample irradiated with the energy range 40–50 keV, sp^2 carbon phases are reduced drastically (9.6%) and oxygen related functional groups are also decreased slightly (21.4%). The apparent increase in the sp^3 carbon phases with the increase of ion beam energy is due to higher

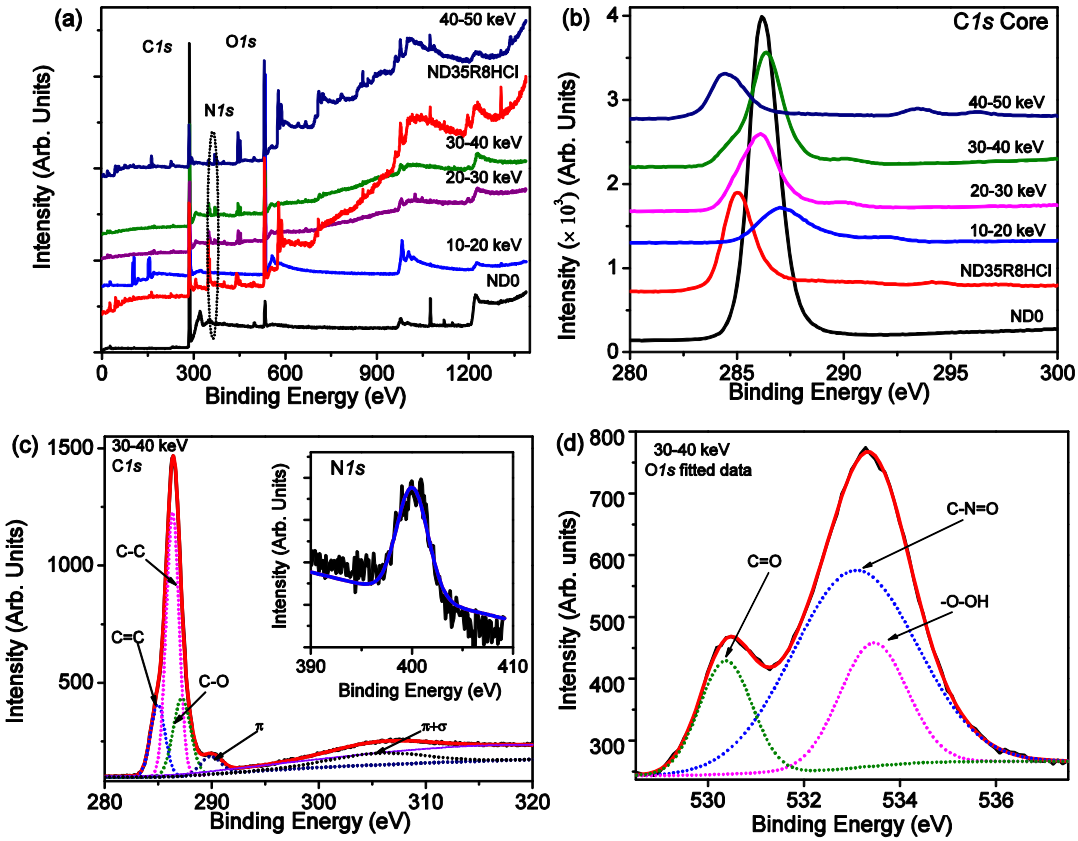

Figure 3. XPS spectra of different NDs. (a) shows the survey scan for initial NDs (ND0) and different irradiated NDs. Survey scan shows the feeble presence of nitrogen in addition to the presence of carbon and oxygen. (b) Shows the C*1s* core spectra of different NDs. (c) shows the fitted C*1s* peak for 30–40 keV sample. Fitting shows the presence of sp^2 carbon in addition to diamond sp^3 phase. Inset shows the N1*s* fitted peak for the same sample. Other samples have been fitted in the same way. (d) Shows the fitted O1*s* core spectra for sample irradiated with 30–40 keV.

electronic energy losses and dispersive nature of the vacancies and defects. The dispersive vacancy profile is not detrimental to diamond phase upon vacuum annealing. For lower ion beam energy, high vacancy concentration profile with the narrow distribution region leads to the phase change and defects near the surface of NDs. As far as the crystallinity of NDs near the surface is concerned, energy range 40–50 keV comes out to be optimized dose. Phase change is minimum in this range and XPS probe depth mainly contains sp^3 carbon phases and oxygen related functional groups which effectively enhance the photo stability of NV^- centers. Inset of figure 3(c) shows the fitted data of N1*s* core (400.9 eV) for sample irradiated with 30–40 keV (table S4, supplementary information). The nitrogen atoms are covalently attached with carbon (C–N). The presence of nitrogen is very small within the probe depth of XPS. Hence, nitrogen atoms are mainly placed near the center of the crystallite. Figure 3(d) shows O1*s* core spectra for different NDs. Initial NDs (ND0) have negligible presence of oxygen near the outer surface. These functional groups include ester and carboxylic acid groups (C=O at 531.4 eV). In addition to this some nitrosyl (533.6 eV) and hydroperoxide (–O–OH at 536.3 eV) groups are present near the outer surface [46]. For refluxed sample (ND35R8HCl), C=O (531.0 eV) and nitrosyl (532.5 eV) bonds are enhanced and hydroperoxide groups are disappeared. For different irradiated NDs, mainly C=O and nitrosyl species are present near the surface. All of these functional groups have the presence of electron donating (oxygen and nitrogen) at outer surface. It leads to electron donating surface and nearby NV^- centers becomes more stable. Hence air oxidation after vacuum annealing is crucial for stability of emission from NDs. The ion irradiated NDs have functional groups in the form of carboxylic, ester (C=O) and nitrosyl moieties with some variation in the position of binding energy attributed to the heterogeneous chemical environment for different samples. Sample irradiated with energy range 40–50 keV have maximum functionalization with C=O moieties. This is advantageous for the preferential fabrication of NV^- centers as far as surface is concerned.

Figure 4(a) shows the fluorescence spectra ($\lambda_{ex} = 514$ nm) for different NDs in the wavelength range 550–750 nm. The emission spectra of different NDs have been fitted with Guassian line shape. As received (ND0) and purified NDs (ND35R8HCl) exhibit weak broad emission in 550–750 nm range. Hence none of these non-irradiated samples contains NV color centers. Also, the irradiated and unannealed NDs (figure S3, supplementary information) exhibit the broad emission band from 520–750 nm. No characteristic emission

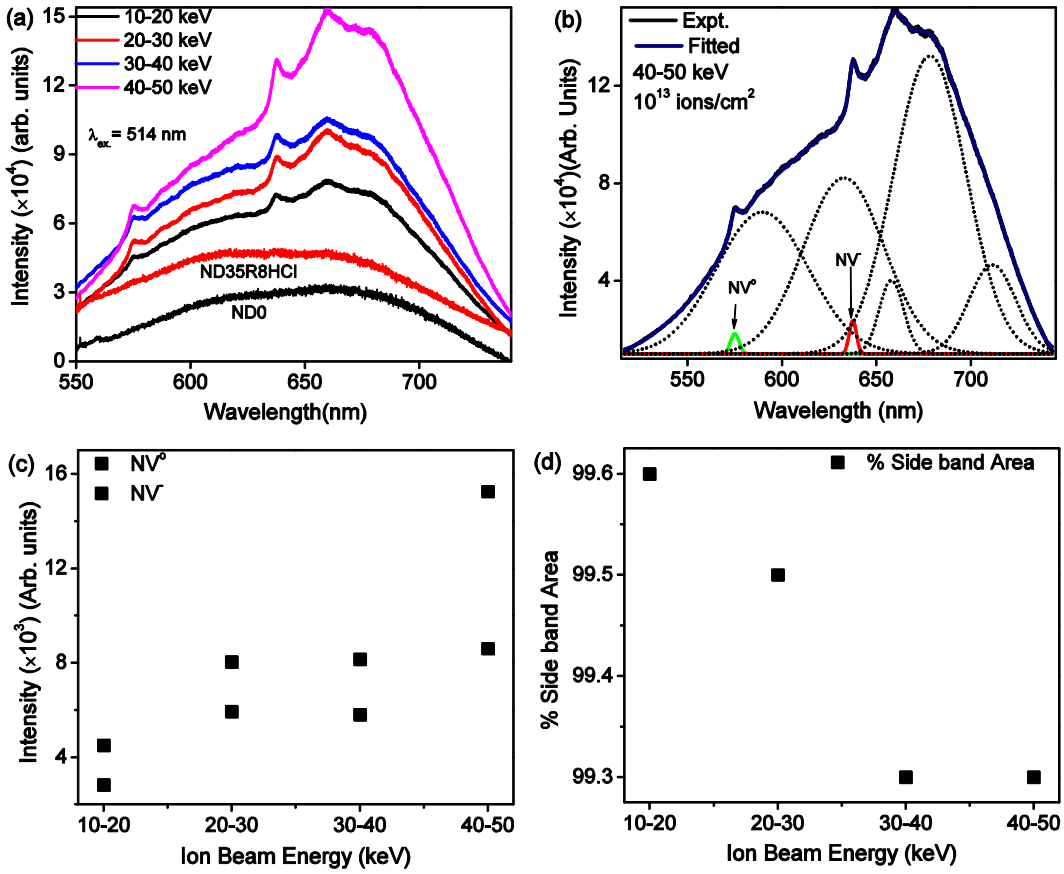

Figure 4. (a) Fluorescence spectra of as received (ND0), purified (ND35R8HCl) and samples irradiated with energy range 10–20 keV, 20–30 keV, 30–40 keV and 40–50 keV. Excitation wavelength for the emission spectra is 514 nm. Fluorescence spectra of ion irradiated samples were taken after vacuum annealing (750 °C, 2 h). The emission intensity of ND0 and ND35R8HCl are increased by an order of 5 for visible comparison. ND0 and ND35R8HCl only exhibit broad emission in 550–750 nm and do not show the characteristic emission from NV centers. (b) Shows the fitted data (Guassian line shape) for sample irradiated with ion energy of 40–50 keV. Characteristic zero phonon line (ZPL) of NV^o (575.1 nm) and NV^- centers (637.8 nm) are seen in addition to broad emission in wavelength range of 550–750 nm. (c) Shows the relative emission intensity of NV^o and NV^- centers in ZPL for different irradiated samples. (d) Shows the percentage side band emission for different ion irradiated NDs.

from NV centers is observed. The observed broad emission is owing to sp^2 carbon phases present at the outer surface of irradiated NDs as confirmed from Raman spectra (figure 2(b)). The vacuum annealing leads to the migration of vacancies and formation of thermally stable NV centers. Different ion irradiated, vacuum annealed and air oxidized NDs exhibit characteristic emission from NV centers as seen in figure 4(a). Different samples contain varying emission intensity of vibronic side bands from NV centers. This varying side band intensity is due to different concentration of NV centers for different samples. Sample irradiated with energy range 10–20 keV have minimum emission intensity and 40–50 keV have the maximum emission in side bands. Further, the emission intensity between ZPL of NV^o and NV^- centers (580–630 nm) is much suppressed in case of sample irradiated with energy range 40–50 keV. Hence the side band of NV^o centers is minimum to this sample. Figure 4(b) shows the fitted peaks for sample irradiated with energy range of 40–50 keV. All the remaining samples have been fitted and correlated in the same way (table S5: supplementary information). Sample irradiated with energy range 10–20 keV shows the characteristic ZPL emission from NV^o (574.8 nm) and NV^- (637.3 nm) centers. In addition to NV^o and NV^- centers, the fitted data for this sample shows the presence of sharp emission features at 658.5 nm (1.882 eV) with the FWHM of 9.3 nm. These emission features are not related with triplet to triplet transition of NV^- centers since threshold energy for band to band excitation/de-excitation in NV^- centers is 1.945 eV. Lower emission from sample irradiated with energy range 10–20 keV is mainly due to high nuclear energy losses near the surface and piling up of large concentration of vacancies in small sample thickness as observed by SRIM simulation (figure S1(a)). High concentration of vacancies leads to their migration at the surface or higher concentration of NV^o centers. Phase change may also take place due to high concentration of vacancies and inefficiency of thermal treatment to restore the crystallinity in the locality of defects as independently confirmed by Raman and XPS. Sample irradiated with energy range 20–30 keV exhibits characteristic ZPL from NV^o (575.2 nm) and NV^- centers (638.0 nm). The side band intensity for this sample is

higher as compared to sample irradiated with the energy range 10–20 keV. This sample also exhibits the sharp emission features in the vibronic side band of NV^- centers at 658.2 nm (1.884 eV) with a FWHM of 10.7 nm. Emission collection is higher due to better dispersion of vacancies (figure 1(c) and table 1). Also, defects and sp^2 phases are suppressed near the surface as confirmed by XPS. This improves the emission collection of NV centers. Sample irradiated with energy range 30–40 keV shows the sharp ZPLs for NV^o (575.4 nm) and NV^- centers (638.3 nm) in addition to their vibronic side band (550–750 nm). Whereas the emission pattern is same, the relative intensity of emission for this energy range is higher as compared to previous samples. This sample also contains sharp emission features at 658.0 nm (1.884 eV) with a FWHM of 9.0 nm. Sample irradiated with energy range 40–50 keV contains characteristic ZPLs of NV^o (575.1 nm) and NV^- centers (637.8 nm) in addition to broad side band emission (figure 4(b)). This irradiated sample also shows sharp emission features at 658.6 nm (1.883 eV) with a FWHM of 9.1 nm. Maximum emission collection for sample irradiated with energy range of 40–50 keV is due to disperse nature of vacancy creation (table 1). Higher concentration of NV^- centers was created with lower probability of annihilation of vacancies to the surface. Further, the oxygen functionalization is maximum for this sample as revealed by XPS. Oxygen provides extra stability to the NV^- centers near the surface as excitons are not being trapped at the surface upon excitation. Figure 4(c) shows the relative emission intensity in ZPLs of NV^o and NV^- for different irradiated samples. It is clear from the figure that the emission intensity of NV^- centers is always larger as compared to NV^o centers in all the irradiated samples. Hence all of these low energy ion irradiation conditions favor the formation of NV^- centers over NV^o centers. But the contrast between the relative intensity of NV^- and NV^o centers is highest for sample irradiated at energy range 40–50 keV. This trend shows that extra electrons for the formation of NV^- centers are easily accessible for this energy range. Extra electrons from substitutional nitrogen atoms (N_s) are more easily accessible for NV centers near the center of crystallite. Because, extra electrons are trapped by the surface defects and NV^o centers are formed in majority near the surface. Hence this energy range (40–50 keV) leads to the prefrable formation of NV^- centers near the center of crystallites and NV^o centers near the surface. This is favorable position for the creation of NV^-centers as the perturbations due to the fact that surface anomalies are minimum at the center and color centers behaves as if they are situated in infinite crystalline array. Figure 4(d) shows the percentage side band emission for different ion irradiated samples. Sample irradiated with energy range 10–20 keV shows 99.6% of total emission in side bands. This shows high electron phonon interaction at room temperature for NV centers. The sample irradiated with energy range 20–30 keV exhibits 99.5% of total emission in side bands. Samples irradiated with energy range 30–40 keV and 40–50 keV shows 99.3% of total emission in side bands of NV centers. Higher emission collection in ZPL is preferable for nano-photonics applications. Hence sample irradiated with 40–50 keV is found to have maximum emission collection and highest contrast between the concentration of NV^- and NV^o centers. These properties are perfectly suitable for different bio-imaging and bio-sensing applications. Higher NV^- centers concentration is also favorable for ensemble magnetometry applications. This makes ion-irradiation in energy range of 40–50 keV (10^{13} ions cm^{-2}) optimized ion dose for the creation of maximum emission from NV centers in HPHT grown NDs.

To confirm the creation of uniform concentration of NV centers, confocal microscopy of different NDs was carried out (figure S4, supplementary information). Figure S4 shows the confocal microscopic images for different ion irradiated, vacuum annealed and air oxidized NDs upon 532 nm laser excitation with the collection window of 570–670 nm. Sample irradiated at lower energy range (10–20 keV) have agglomeration of NDs particles as observed in bright field image (figure S4(b)). Emission from NV centers is mostly observed in agglomerated area of sample. Dispersed portion of sample has very feeble emission intensity. This shows the lower emission collection from NV centers in this sample. The lower emission intensity is due to lower concentration of NV centers due to limited penetration of He^+ ions. Further, the emission from NV centers is quenched due to presence of defects owing to ion-irradiation (as evident from Raman and XPS). Brightness and dispersion have been improved for sample irradiated with energy range 20–30 KeV as shown in figures S4(c) and S4(d). The brightness is increased owing to higher concentration of NV centers and dispersed nature of He^+ ions (SRIM, table 1(a)). Defects are reduced and oxygen functional groups have been improved at the outer surface as confirmed by XPS. The brightness has been further improved (figure S4(e)) in the dispersed NDs (figure S4(f)). Maximum brightness from NDs is achieved from sample irradiated with 40–50 keV. This sample has maximum emission collection from NV centers as previously confirmed by emission spectra (figure 4). The emission is uniformly distributed over the whole sample. The uniform brightness dispersion demonstrates the creation of uniform concentration of NV centers. These ion irradiation conditions are optimized fabrication conditions for the creation of NV centers in HPHT NDs (Type Ib, $N_s \sim 100$ ppm). If the concentration of nitrogen (N_s) is higher (lower) than ~100 ppm, the energy range will be same but the ion dose (fluence) will be higher (lower).

Figures 5(a)–(c) shows the images obtained from ND35R8HCl-**50 keV** (10^{13} dose): sample irradiated with mono-energetic beam [39] and figures (d)–(f) shows images from ND35R8HCl **40–50 keV** (10^{13} dose): sample irradiated with beam having three different energy 40–50 keV (40 keV, 45 keV and 50 keV) and same fluence

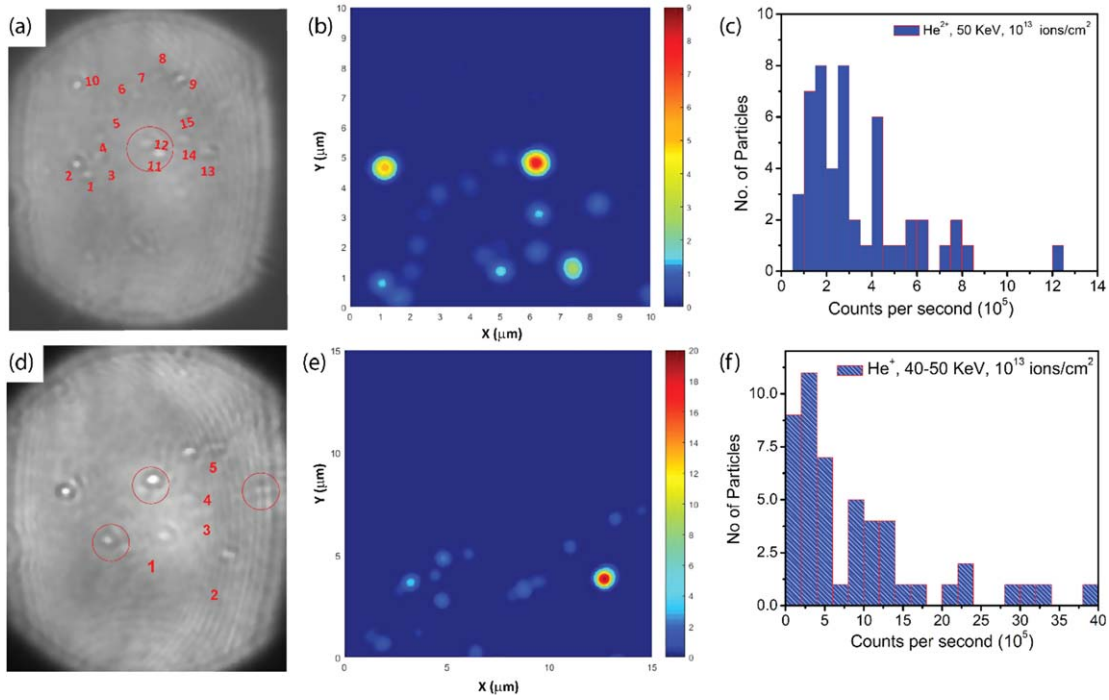

Figure 5. Optical micrograph and statistical analysis of emission from individual emission centers of ND35R8HCl-**50 keV** (10^{13} dose) figures (a)–(c) and ND35R8HCl **40–50 keV** 10^{13} dose figures (d)–(f).

(10^{13} ions cm^{-2}). Figures 5(a) and (d) shows the widefield micrograph, while confocal fluorescence micrograph ($\lambda_{ex} = 532$ nm) is shown in figures 5(b) and (e) respectively. By masking at the back focal plane the emission from individual particles were recorded. Count rates in the histogram for ND35R8HCl-**50 keV and** ND35R8HCl **40–50 keV** is shown after background count correction. Sample created with monoenergetic beam irradiation (ND35R8HCl-50 KeV (10^{13} dose)) shows emission rates in the range (0.5–13)$\times 10^5$ counts per second with majority of them emitting at (2–3)$\times 10^5$ counts per second. Whereas, in case of sample irradiated with varying energy in the range 40–50 KeV for the same dose (ND35R8HCl 40–50 KeV 10^{13}) shows counts in the range (2.5–5) $\times 10^5$ counts per second. Moreover, out of 50 particles monitored, the distribution of particles in case of varying energy experiment was narrow over the emission rates, while in monoenergetic irradiation emission rate is spread over the particles. So through controlled experiments, we have been able to create brighter and uniform emission from nanodiamonds.

Conclusion

We have successfully fabricated the uniform concentration of NV centers in type Ib NDs by low energy ion irradiation and using distributed ion energy range. The ion beam energy range was carefully investigated by using SRIM calculations. Ion irradiation leads to defects generation near the surface but the crystallinity was intact upon ion irradiation and vacuum annealing. The crystallite size was found to be reduced up to some extent owing to phase change near the surface during ion irradiation. Oxygen related functional groups (carboxylic, ester and peroxide) and some nitrogen related moieties were attached near the surface by post annealing air oxidation. These oxygen related functional groups effectively removes the defects from the outer surface (XPS) and thus enhance the emission collection of NV centers. Sample irradiated with energy range 40–50 keV is found to have maximum ensemble emission collection from NV centers. Apart from this, the maximum ZPL contrast between NV^- and NV^o centers is achieved for this sample. Also, the side band emission from NV^- centers (650–750 nm) is maximum for this sample. Confocal microscopy reveals that sample irradiated with the energy range 40–50 keV have brightest and uniform emission throughout the sample. The ion irradiation at 40–50 keV and dose of 10^{13} ions cm^{-2} is the optimized ion implantation condition for uniform and bright emission from NDs. Our work provides the efficient, commercial and straight forward root for the fabrication of uniformly distributed NV centers. The method to fabricate uniformly bright NDs reported in this work would accelerate the use of fluorescent NDs for bio-imaging, bio-sensing and ensemble magnetometry.

Acknowledgments

Dilip K Singh thanks DST, Govt. of India for financial support through Inspire faculty award (IFA-13 PH-65). Ravi Kumar thanks CSIR, New Delhi for providing SRF Fellowship.

ORCID iDs

Tai Trinh Cong https://orcid.org/0000-0002-1642-4313
Prabir Pal https://orcid.org/0000-0002-7356-2587
S R Dhakate https://orcid.org/0000-0003-2463-9792
Dilip K Singh https://orcid.org/0000-0002-8162-7766

References

[1] Aharonovich I, Castelletto S, Simpson D, Su C, Greentree A and Prawer S 2011 Diamond-based single-photon emitters *Rep. Prog. Phys.* **74** 076501
[2] Mochalin V N, Shenderova O, Ho D and Gogotsi Y 2012 The properties and applications of nanodiamonds *Nat. Nanotechnol.* **7** 11–23
[3] Kaur R and Badea I 2013 Nanodiamonds as novel nanomaterials for biomedical applications: drug delivery and imaging systems *Int. J. Nanomed.* **8** 203–220
[4] Vaijayanthimala V and Chang H 2009 Functionalized fluorescent nanodiamonds for biomedical applications *Nanomedicine* **4** 47–55
[5] Schirhagl R, Chang K, Loretz M and Degen C L 2014 Nitrogen-vacancy centers in diamond: nanoscale sensors for physics and biology *Annu. Rev. Phys. Chem.* **65** 83–105
[6] Wrachtrup J and Jelezko F 2006 Processing quantum information in diamond *J. Phys. Condens. Matter* **18** S807
[7] Schrand A M, Dai L, Schlager J J, Hussain S M and Osawa E 2007 Differential biocompatibility of carbon nanotubes and nanodiamonds *Diamond Relat. Mater.* **16** 2118–23
[8] Schrand A M, Huang H, Carlson C, Schlager J J, Ōsawa E, Hussain S M and Dai L 2007 Are diamond nanoparticles cytotoxic? *J. Phys. Chem.* B **111** 2–7
[9] Chang B M *et al* 2013 Highly fluorescent nanodiamonds protein-functionalized for cell labeling and targeting *Adv. Funct. Mater.* **23** 5737–45
[10] Fu C-C *et al* 2007 Characterization and application of single fluorescent nanodiamonds as cellular biomarkers *Proc. Natl Acad. Sci.* **104** 727–32
[11] Doherty M W, Manson N B, Delaney P, Jelezko F, Wrachtrup J and Hollenberg L C 2013 The nitrogen-vacancy colour centre in diamond *Phys. Rep.* **528** 1–45
[12] Rondin L *et al* 2010 Surface-induced charge state conversion of nitrogen-vacancy defects in nanodiamonds *Phys. Rev.* B **82** 115449
[13] Hauf M *et al* 2011 Chemical control of the charge state of nitrogen-vacancy centers in diamond *Phys. Rev.* B **83** 081304
[14] Yamano H *et al* 2017 Charge state stabilization of shallow nitrogen vacancy centers in diamond by oxygen surface modification *Japan. J. Appl. Phys.* **56** 04CK08
[15] Collins A, Thomaz M and Jorge M I B 1983 Luminescence decay time of the 1.945 eV centre in type Ib diamond *J. Phys. C: Solid State Phys.* **16** 2177
[16] Holt K B 2007 Diamond at the nanoscale: applications of diamond nanoparticles from cellular biomarkers to quantum computing *Philosophical Transactions of the Royal Society of London A: Mathematical, Physical and Engineering Sciences* **365** 2845–61
[17] Billinton N and Knight A W 2001 Seeing the wood through the trees: a review of techniques for distinguishing green fluorescent protein from endogenous autofluorescence *Anal. Biochem.* **291** 175–97
[18] Lim Y T, Kim S, Nakayama A, Stott N E, Bawendi M G and Frangioni J V 2003 Selection of quantum dot wavelengths for biomedical assays and imaging *Molecular Imaging* **2** 15353500200302163
[19] Kurtsiefer C, Mayer S, Zarda P and Weinfurter H 2000 Stable solid-state source of single photons *Phys. Rev. Lett.* **85** 290
[20] Yu S-J, Kang M-W, Chang H-C, Chen K-M and Yu Y-C 2005 Bright fluorescent nanodiamonds: no photobleaching and low cytotoxicity *JACS* **127** 17604–5
[21] Mohan N, Chen C-S, Hsieh H-H, Wu Y-C and Chang H-C 2010 *In vivo* imaging and toxicity assessments of fluorescent nanodiamonds in Caenorhabditis elegans *Nano Lett.* **10** 3692–9
[22] Tisler J *et al* 2011 Highly efficient FRET from a single nitrogen-vacancy center in nanodiamonds to a single organic molecule *ACS Nano* **5** 7893–8
[23] Mohan N *et al* 2010 Sub-20-nm fluorescent nanodiamonds as photostable biolabels and fluorescence resonance energy transfer donors *Adv. Mater.* **22** 843–7
[24] van Oort E, Stroomer P and Glasbeek M 1990 Low-field optically detected magnetic resonance of a coupled triplet-doublet defect pair in diamond *Phys. Rev.* B **42** 8605
[25] Gruber A, Dräbenstedt A, Tietz C, Fleury L, Wrachtrup J and Von Borczyskowski C 1997 Scanning confocal optical microscopy and magnetic resonance on single defect centers *Science* **276** 2012–4
[26] Loretz M, Takahashi H, Segawa T F, Boss J M and Degen C L 2017 Optical hyperpolarization of nitrogen donor spins in bulk diamond *Phys. Rev.* B **95** 064413
[27] Baranov P G *et al* 2011 Enormously high concentrations of fluorescent nitrogen-vacancy centers fabricated by sintering of detonation nanodiamonds *Small* **7** 1533–7
[28] Rabeau J *et al* 2007 Single nitrogen vacancy centers in chemical vapor deposited diamond nanocrystals *Nano Lett.* **7** 3433–7
[29] Walker J 1979 Optical absorption and luminescence in diamond *Rep. Prog. Phys.* **42** 1605
[30] Boudou J-P *et al* 2009 High yield fabrication of fluorescent nanodiamonds *Nanotechnology* **20** 235602
[31] Iakoubovskii K and Adriaenssens G J 2001 Trapping of vacancies by defects in diamond *J. Phys. Condens. Matter* **13** 6015
[32] Smith B R *et al* 2009 Five-nanometer diamond with luminescent nitrogen-vacancy defect centers *Small* **5** 1649–53
[33] Wee T-L *et al* 2007 Two-photon excited fluorescence of nitrogen-vacancy centers in proton-irradiated type Ib diamond *J. Phys. Chem.* A **111** 9379–86

[34] Chang Y-R *et al* 2008 Mass production and dynamic imaging of fluorescent nanodiamonds *Nat. Nanotechnol.* **3** 284–8
[35] Su L-J *et al* 2013 Creation of high density ensembles of nitrogen-vacancy centers in nitrogen-rich type Ib nanodiamonds *Nanotechnology* **24** 315702
[36] Wee T-L, Mau Y-W, Fang C-Y, Hsu H-L, Han C-C and Chang H-C 2009 Preparation and characterization of green fluorescent nanodiamonds for biological applications *Diamond Relat. Mater.* **18** 567–73
[37] Havlik J *et al* 2013 Boosting nanodiamond fluorescence: towards development of brighter probes *Nanoscale* **5** 3208
[38] Stursa J *et al* 2016 Mass production of fluorescent nanodiamonds with a narrow emission intensity distribution *Carbon* **96** 812–8
[39] Kumar R, Yoon S J, Lee K G, Pal P, Pant R P, Suman C K, Dhakate S R, Kumar R, Avasthi D K and Singh D K 2016 Purification method dependent fluorescence from nitrogen-vacancy (NV) centers of nano-diamonds *RSC Adv.* **6** 47164–73
[40] Kumar R, Pandit P, Pal P, Dhakate S R, Pant R P, Kumar R, Avasthi D K and Singh D K 2018 Bright fluorescent nano-diamonds through optimized engineering of nitrogen-vacancy (NV) centers *AIP Adv.* **8** 085023
[41] Osswald S, Yushin G, Mochalin V, Kucheyev S O and Gogotsi Y 2006 Control of sp^2/sp^3 carbon ratio and surface chemistry of nanodiamond powders by selective oxidation in air *J. Am. Chem. Soc.* **128** 11635
[42] Ziegler J F and Biersack J P 1985 The stopping and range of ions in matter *Treatise on Heavy-Ion Science* (Berlin: Springer) (https://doi.org/10.1007/978-1-4615-8103-1_3)
[43] Koike J, Parkin D and Mitchell T 1992 Displacement threshold energy for type IIa diamond *Appl. Phys. Lett.* **60** 1450–2
[44] Holzwarth U and Gibson N 2011 The Scherrer equation versus the 'Debye–Scherrer equation' *Nat. Nanotechnol.* **6** 534–534
[45] Cui S and Hu E L 2013 Increased negatively charged nitrogen-vacancy centers in fluorinated diamond *Appl. Phys. Lett.* **103** 051603
[46] Cunningham G, Panich A, Shames A, Petrov I and Shenderova O 2008 Ozone-modified detonation nanodiamonds *Diamond Relat. Mater.* **17** 650–4